

THE UNUSUAL X-RAY BINARIES OF THE GLOBULAR CLUSTER NGC 6652

G. COOMBER¹, C. O. HEINKE^{1,2}, H. N. COHN³, P. M. LUGGER³, J. E. GRINDLAY⁴*Draft version November 23, 2018*

ABSTRACT

Our 5 ks *Chandra* ACIS-S observation of the globular cluster NGC 6652 detected 7 X-ray sources, 3 of which are previously unidentified. This cluster hosts a well-known bright low-mass X-ray binary, source A (or XB 1832-330). Source B shows unusual rapid flaring variability, with an average L_X (0.5–10 keV) $\sim 2 \times 10^{34}$ ergs/s, but with minutes-long flares up to $L_X = 9 \times 10^{34}$ ergs/s. Its spectrum can be fit by an absorbed power-law of photon index $\Gamma \sim 1.24$, and hardens as the countrate decreases. This suggests that part or all of the variation might be due to obscuration by the rim of a highly inclined accretion disk. Sources C and D, with $L_X \sim 10^{33}$ ergs/s, have soft and unusual spectra. Source C requires a very soft component, with a spectrum peaking at 0.5 keV, which might be the hot polar cap of a magnetically accreting polar cataclysmic variable. Source D shows a soft spectrum (fit by a power-law of photon index ~ 2.3) with marginal evidence for an emission line around 1 keV; its nature is unclear. The faint new sources E, F, and G have luminosities of $1\text{--}2 \times 10^{32}$ ergs/s, if associated with the cluster (which is likely). E and F have relatively hard spectra (consistent with power-laws with photon index ~ 1.5). G lacks soft photons, suggesting absorption with $N_H > 10^{22}$ cm⁻².

Subject headings: binaries : X-rays — stars: neutron — cataclysmic variables — globular clusters (individual): NGC 6652

1. INTRODUCTION

The high-density environments of globular clusters were suggested to be causes of X-ray binary production early in X-ray astronomy (Katz 1975; Clark 1975). Several types of X-ray sources have now been identified in Galactic globular clusters (Verbunt & Lewin 2004). Fifteen luminous low-mass X-ray binaries (LMXBs) reach $L_X > 10^{35}$ ergs/s, some only during short outbursts (Sidoli et al. 2001; Verbunt & Lewin 2004; Heinke et al. 2010; Pooley et al. 2010). The low-luminosity X-ray sources $L_X = 10^{29}$ – 10^{34} ergs/s include several types of systems such as quiescent LMXBs (containing neutron stars between accretion episodes), millisecond radio pulsars, cataclysmic variables (CVs), and magnetically active binaries (Verbunt & Lewin 2004). Quiescent LMXBs containing neutron stars (qLMXBs) often show soft thermal spectra dominated by blackbody-like emission (Rutledge et al. 2002a; Heinke et al. 2003), though a spectrally harder component is often present and sometimes dominant (Campana et al. 2002; Jonker et al. 2004b; Wijnands et al. 2005). The origin of the soft component is generally thought to be thermal X-ray emission from the heated NS surface, modified by the star’s hydrogen atmosphere (Zavlin et al. 1996; Brown et al. 1998). The harder power-law component is not yet well understood, but may be produced by continuing accretion or possibly pulsar activity (Campana et al. 1998).

The globular cluster NGC 6652 contains one luminous ($L_X > 10^{36}$) LMXB, XB 1832-330 (Predehl et al. 1991)

and several lower-luminosity X-ray sources. This core-collapsed (Noyola & Gebhardt 2006) cluster is ~ 11.7 Gyr old (Chaboyer et al. 2000), 9.0 ± 0.4 kpc from the sun and suffers extinction with equivalent hydrogen column density $N_H = 5.0 \times 10^{20}$ cm⁻² (Harris 1996). The three fainter sources detected by Heinke et al. (2001) in a 1.6 ks *Chandra* HRC-I observation are not well understood. The brightest of the three low- L_X sources (source B) was seen at luminosities of a few 10^{33} ergs/s while its optical counterpart lies on the main sequence (1 magnitude below the turnoff) in a $V - I$ optical color-magnitude diagram, suggesting a qLMXB nature (Heinke et al. 2001). However, the optical counterpart has also been observed to show blue $U - V$ colors (Deutsch et al. 1998), and strong variability with a (possible) 43.6-minute period (Deutsch et al. 2000), which, if it is the true period, would exclude a main-sequence companion. Source C has a very blue optical counterpart, which indicates a bright disk and a relatively high rate of mass transfer. Combining this with its relatively low L_X , the efficiency of energy extraction is inferred to be relatively low, suggesting a CV rather than an LMXB (Heinke et al. 2001).

In this paper we present a 2008 *Chandra* ACIS-S observation of NGC 6652’s X-ray sources. We also consult 2000 *Chandra* HRC-I data and 1994 ROSAT HRI data for long-term variability information.

2. DATA REDUCTION

We observed NGC 6652 on June 9, 2008 for 5.6 ks with *Chandra*’s ACIS-S detector in a 1/4 subarray mode. The data were reduced using the CIAO version 4.3 software⁵. We created a new bad pixel file with the `acis_run_hotpix` script. The level 1 event files were reprocessed by calibrating for charge-transfer inefficiency

¹ University of Alberta, Dept. of Physics, 11322-89 Avenue, Edmonton AB T6G 2G7, Canada

² Ingenuity New Faculty; heinke@ualberta.ca

³ Dept. of Astronomy, Indiana University, 727 East 3rd St., Bloomington IN 47405, USA

⁴ Harvard-Smithsonian Center for Astrophysics, 60 Garden Street, Cambridge MA 02138, USA

⁵ Available at <http://cxc.harvard.edu/ciao/>

on the detector and time-dependent gain adjustments. The data was then filtered for grade and status bits according to the standard CIAO Science Threads⁶. A background light curve shows no evidence of flaring.

The CIAO WAVDETECT program was run using the energy range 0.3-7.0 keV. We find 7 sources, all of which are located within (or at) the cluster half-mass radius r_h , 0'.65 (Harris 1996). Three faint sources (E, F and G) were not visible in the HRC observation of NGC 6652 by Heinke et al. (2001). The positions of sources B through G, shown in Table 1, were computed using WAVDETECT centroiding. Due to the high flux of photons from source A, pileup effects produce a characteristic “donut hole” at the source location and a prominent readout streak, which prevents WAVDETECT from accurately computing the position of source A. We therefore estimated the location of source A by matching a symmetric circle to the “donut hole”, by eye. Running WAVDETECT in the energy bands 0.3-2.0 keV, 2.0-5.0 keV, and 5.0-7.0 keV did not locate additional sources. The positions of sources A, B, C and D are consistent with those from the 2001 *Chandra* observation. We show a smoothed ACIS image of NGC 6652 in Fig. 1. Using the log N-log S relationship of Giacconi et al. (2001), we calculated the expected number of active galactic nuclei observed within one half-mass radius of the cluster to be 0.14, indicating that all detected X-ray sources are likely to be members of the cluster.

Due to pileup effects, the data from the source region of A is not reliable. Pileup occurs when two or more photons are recorded by the CCD as a single higher energy event, which results in distortion of the observed source spectrum and an underestimated count rate (Davis 2001). The high count rate also produces a readout streak, as photons land on the detector during the short frame readout time. By extracting a spectrum from the readout streak, we are able to obtain spectral data from source A without having to model the pileup. Using `dmextract` we extract a source spectrum from the readout streak, and a background spectrum from surrounding source-free regions of the observation. We then create new RMF and ARF files using the tools `mkacisrmf` and `mkarf` respectively, and correct the streak exposure time to 110.4 s to account for the fact that the spectrum was extracted from the ACIS readout streak.

For sources B, C and D, we extracted 0-10 keV spectra using `specextract` from circular regions, of radius 2" for B and 1.4" for C and D, located at the source positions produced by WAVDETECT. We produced spectra, response files and backgrounds following the appropriate CIAO thread⁷, correcting the response files for the fraction of the flux contained within the extraction aperture, group the spectra, and fit them within XSPEC⁸. Count rates were calculated for sources E, F and G directly from the level 2 event file using the `dmstat` tool, since these sources are too faint to allow spectral analysis. The count rates were then converted into unabsorbed fluxes with PIMMS⁹, by assuming that the faint source spectra can be modeled by a power law of photon index Γ

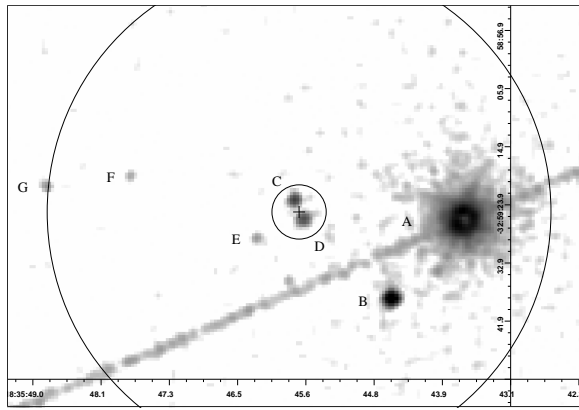


FIG. 1.— *Chandra* ACIS-S image of NGC 6652. The data is smoothed with a gaussian kernel radius of 1". The 7 detected sources are labeled from A to G. Both the core radius (0.07') and the half mass radius (0.65') are indicated.

$= 1.4$, typical for globular cluster sources at this L_X (Heinke et al. 2005), and consistent with their hardness ratios (below).

To study long term variability of the sources, we re-analyze the archival HRC-I data from a 2000 observation of NGC 6652, filtering the data for grade and status. We extract lightcurves for sources A, B, C, and D with the CIAO tool `dmextract` and estimate source luminosities with PIMMS. We extract counts and lightcurves from source regions of radius 2" centered at the WAVDETECT coordinates obtained from our ACIS observation.

3. X-RAY ANALYSIS

3.1. Source A

The 462 events extracted from source A's readout streak were grouped into 9 bins, with 50 counts per bin to maximize spectral resolution while minimizing the error in the normalized counts in each bin (Fig. 2). We ignore events above 8 keV, as the ACIS response is poorly understood at these energies. The spectrum is well fit by an absorbed power-law model with a photon index of $\Gamma = 1.7^{+0.3}_{-0.2}$ (Table 2). The N_H value of $2.7^{+0.1}_{-0.1} \times 10^{21} \text{ cm}^{-2}$ exceeds the accepted cluster value of $5 \times 10^{20} \text{ cm}^{-2}$ (Harris 1996). We derive an unabsorbed luminosity for source A of $L_X(0.5-6.0) = 4.4^{+0.6}_{-0.5} \times 10^{35} \text{ ergs/s}$. Mukai & Smale (2000) observed XB 1832-330 with ASCA, finding that a partial covering model was required, instead of a single absorption column, to fit the spectrum. A similar model was required by BeppoSAX (Parmar et al. 2001) and XMM (Sidoli et al. 2008) observations. Our spectrum is of insufficient quality to distinguish between a partial covering model vs. a single absorption column.

We detect 9205 counts for source A in the 2000 HRC observation of NGC 6652. We convert the average source count rate into an unabsorbed bolometric X-ray luminosity with PIMMS using our best ACIS spectral fit, finding $L_X(0.5-6.0) = (1.61 \pm 0.02) \times 10^{36} \text{ ergs/s}$. A's luminosity appears to have decreased by almost a factor of four from 2000 to 2008. Sidoli et al. (2008) report two XMM observations in Sept. and Oct. 2006. Converting their X-ray luminosities to the 0.5-6 keV range, they find $L_X(0.5-6 \text{ keV}) = 1.2 \times 10^{36}$ and $1.1 \times 10^{36} \text{ ergs/s}$. Parmar et al. (2001) report a BeppoSAX measurement in March 2001,

⁶ <http://cxc.harvard.edu/ciao/threads/all.html>

⁷ <http://cxc.harvard.edu/ciao/threads/psextract/>

⁸ <http://heasarc.gsfc.nasa.gov/docs/xanadu/xspec/>

⁹ <http://asc.harvard.edu/toolkit/pimms.jsp>

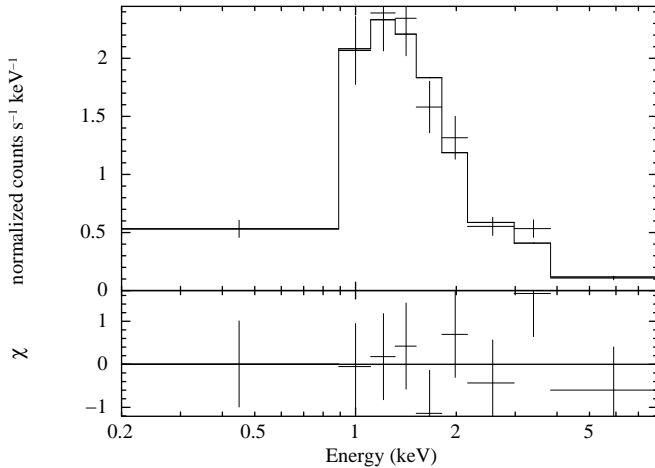


FIG. 2.— Top: *Chandra* 2008 X-ray spectrum of source A containing 9 bins of 50 counts per bin. The spectrum is best-fit by an absorbed power-law model of photon index of $\Gamma = 1.7^{+0.3}_{-0.2}$. Bottom: Residuals to the best fit.

which we convert to $L_X(0.5-6 \text{ keV}) = 1.5 \times 10^{36} \text{ ergs/s}$. Tarana et al. (2007) report 2003-2005 INTEGRAL measurements (restricted to $>20 \text{ keV}$, and thus not directly comparable to our fluxes) that are consistent with the BeppoSAX flux. RXTE PCA Galactic Bulge Scan monitoring of X1832-330¹⁰ indicates substantial variability on ~ 6 -month time scales, but also a general declining trend from 1999 to 2010, by about 30%.

3.2. Source B

3.2.1. Timing Analysis

We produced a lightcurve by binning the 0.3-7 keV data into 103 bins each with 50s per bin (Fig. 3), which shows clear variability, by factors >10 on timescales $<100 \text{ s}$. (A K-S test indicates variability at $>99.9\%$ confidence.) Such variability is unusual in low-mass X-ray binaries. To test whether the variation may be caused by changes in obscuring column (perhaps, if the system is edge-on, caused by material at the rim of an accretion disk), we group the lightcurve by countrate, with boundaries when the countrate crosses 0.15 and 0.3 counts/s (as the count statistics are low for 50 s bins). Within each larger bin, we compute the hardness ratio of 0.3-1 keV photons (the most likely to be absorbed) over 0.3-7 keV photons (Fig. 3, bottom), with binomial 1σ errorbars derived from Gehrels (1986). If the dips were due to obscuration, we might expect the lowest-countrate bins to have the lowest hardness ratios. This is suggested by the first 1000 s, but is less clear from the dataset as a whole. We quantify this by comparing the ratio of 0.3-1 keV counts to total counts in the low-countrate portions ($<0.15 \text{ cts/s}$), vs. medium and high-countrate portions (below and above 0.3 cts/s), finding the fraction to be 0.15 ± 0.03 for the low-countrate portions vs. 0.25 ± 0.04 and 0.23 ± 0.03 for the higher-countrate portions. This is a significant effect, indicating that obscuration may play a role in the dipping.

The peaks in the lightcurve reach countrates that suggest substantial pileup. We estimate the amount of pileup and intrinsic luminosities using the PIMMS tool, for the best-fit absorbed power-law spectrum (see be-

low; the choice of spectrum does not appreciably affect results). At the peak observed countrate of 0.46 cts/s, the estimated fraction of recorded events that are actually multiple is 27%, and we infer the intrinsic $L_X(0.3-7) \sim 9 \times 10^{34} \text{ ergs/s}$, a factor of 2 higher than would be extrapolated without pileup. However, the pileup model in PIMMS is systematically uncertain, so the true peak L_X is uncertain, presumably by less than a factor of 2. The inferred minimum L_X is $< 2 \times 10^{33} \text{ ergs/s}$, for 0.02 cts/s (cf. Fig. 3).

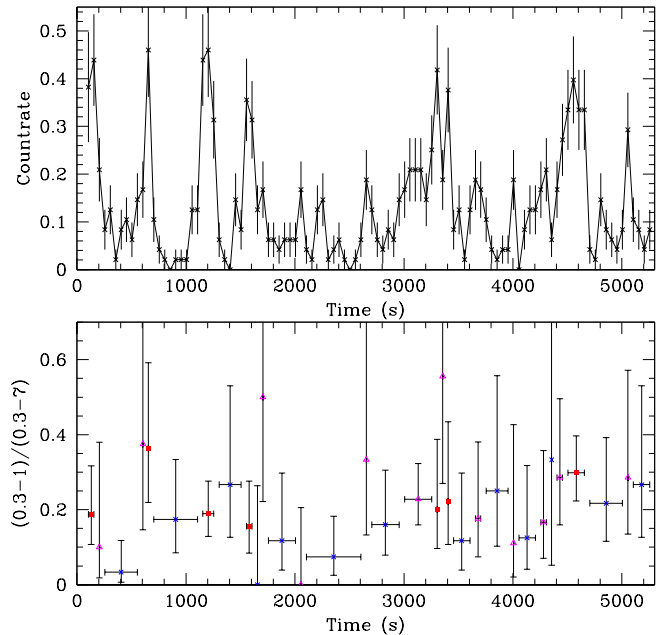


FIG. 3.— Top: ACIS countrate lightcurve of source B, 0.3-7 keV, in 50 s bins. L_X/ctrate conversion estimated as $1.2 \times 10^{34} \text{ ergs/s}$ for 0.1 cts/s, reaching $9 \times 10^{34} \text{ ergs/s}$ for 0.46 cts/s, due to pileup. Bottom: Ratio of counts in 0.3-1 keV vs. those in 0.3-7 keV. Boundaries of ratio bins set by when countrate crosses 0.15 and 0.3 cts/s. Bins over 0.3 cts/s: (red) filled squares; 0.3-0.15 cts/s: (magenta) open triangles; and under 0.15 cts/s: (blue) crosses.

Power spectra (produced using XRONOS¹¹) show no evidence of periodicity during the 5.6 ks ACIS observation. We re-examined the 2000 HRC observation to check for long-term variability. Using PIMMS and our best ACIS spectral fit (below), we estimate the unabsorbed luminosity to be $L_X(0.5-6.0) = (1.1 \pm 0.1) \times 10^{34} \text{ ergs/s}$, vs. our average ACIS unabsorbed luminosity of $L_X(0.5-6.0) = 1.1^{+0.1}_{-0.1} \times 10^{34} \text{ ergs/s}$ (section 3.2.2). Heinke et al. (2001) found significant variability during the HRC observation. The short, low-sensitivity lightcurve suggests variation by at least a factor of two. As the HRC sensitivity and exposure length are each 3 times smaller than those for the ACIS observation, its usefulness for studying variability is limited.

An archival ROSAT HRI observation (March 27, 1994, for 817 s exposure time) shows marginal evidence for source B. The image (Fig. 4) shows one bright source, which we attribute to A, setting our astrometry. We mea-

¹⁰ http://lheawww.gsfc.nasa.gov/users/craigm/galscan/html/R_1832-330.html

¹¹ <http://heasarc.nasa.gov/docs/xanadu/xronos/xronos.html>

sure 6 photons within $2''$ of source B's position, while only $1.4^{+2.5}_{-1}$ photons are expected at this position, using the average background rate between $6.5''$ and $10''$ from source A, giving $4.6^{+1}_{-2.5}$ (at 1 sigma; $4.6^{+1.3}_{-4.6}$ at 2 sigma, Gehrels 1986) photons from B. This $\sim 2\sigma$ detection suggests (correcting for the HRI point-spread function enclosed energy of 38% within $2''$) $L_X(0.5-6 \text{ keV}) = 1.5^{+0.3}_{-0.8} \times 10^{34}$ ergs/s. Thus, we have no evidence for B's variability on long time scales.

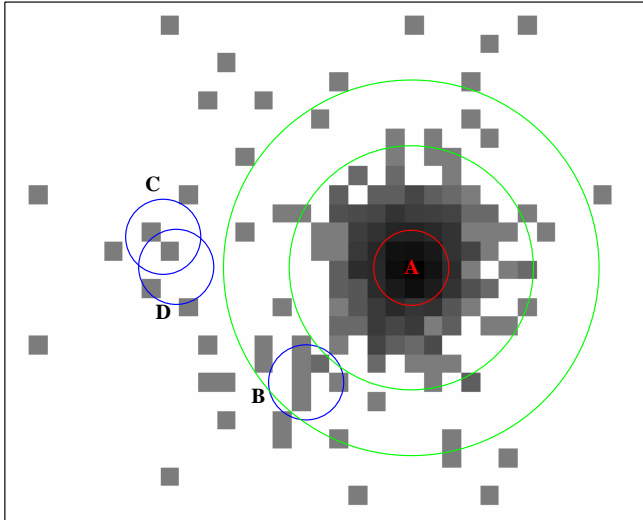


FIG. 4.— ROSAT HRI image, March 1994, of NGC 6652. The (corrected, using A's position) positions of sources A, B, C and D are marked with small (radius= $2''$) circles, while the annulus around A used to estimate the background is indicated with larger circles (radius $6.5''$ and $10''$).

3.2.2. Spectral Analysis

We created both an overall time-averaged spectrum of B (680 counts, binned by 30 counts/bin), and spectra for the three count-rate ranges listed above. We include the Chandra CCD pileup model (Davis 2001), with the grade morphing parameter α fixed to 0.5, and photoelectric absorption (XSPEC *phabs*). B's time-averaged spectrum can be fit well with an absorbed power-law model with photon index $\Gamma = 1.24^{+0.10}_{-0.23}$ (Table 2). We also try adding a NS hydrogen atmosphere model (NSATMOS, Heinke et al. 2006a) to the absorbed power-law model. We fix the mass and radius to canonical values ($1.4 M_\odot$, 10 km), so kT is the only free parameter. The NSATMOS component does not improve the quality of the spectral fit, and the upper limit on its kT implies an upper limit on $L_{X,NS}(0.5-10.0 \text{ keV}) < 7 \times 10^{32}$ ergs/s. This limit may not be applicable if the system is edge-on, as the NS could suffer higher N_H than other X-ray emitting regions.

We next fitted the three count-rate-selected spectra, with 240, 186, and 253 counts [low to high], binned by 15 counts each, to investigate what parameters may be changing. An absorbed, piled-up power-law spectrum is best fit with (at least) two parameters varying; the power-law normalization, and either the N_H or power-law spectral index. We give parameters for both such fits in Table 3. The alternative of allowing only the power-law normalization to vary gives significant residuals in the spectra (Fig. 5), and a higher chi-squared: 42.93 for

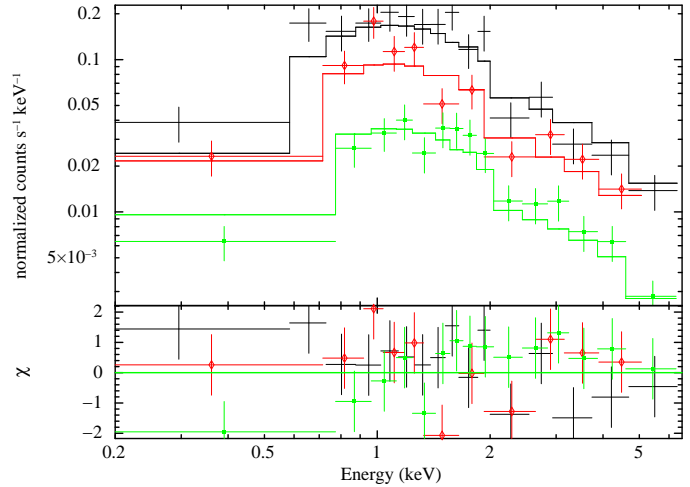


FIG. 5.— Top: *Chandra* X-ray spectra of source B at high (black, crosses), medium (red, diamonds) and low (green, filled squares) count-rates. All are fit with a power-law model with only normalization varying (see text). Bottom: Residuals to this fit, demonstrating the spectral changes.

38 degrees of freedom (dof), vs. 30.3 or 30.6 (for 36 dof) from the other two models (respectively). An F-test gives probabilities of 0.2% of attaining such an improvement in the chi-squared by chance, indicating that another quantity besides the normalization is also varying.

3.3. Source C:

An unbinned 0.3-7 keV lightcurve gives a 0.01 K-S probability of source constancy, indicating that C is variable. This is confirmed by its (0.3-7 keV, 500 s binning) lightcurve, which shows two clear peaks (Fig. 6). A power spectrum shows no evidence of periodicity. Using the best-fit double mekal spectral model (below), we find a peak $L_X(0.5-10.0) = 3.4^{+1.1}_{-1.1} \times 10^{33}$ ergs/s, and a minimum $L_X < 3.2 \times 10^{32}$ ergs/s, for an average $L_X = 1.1 \times 10^{33}$. Using the power-law spectral model (a poor fit) to the ACIS data to infer the HRC spectrum, we find $L_X = 2 \times 10^{32}$ ergs/s, half the ACIS estimate with this spectrum, but the spectral uncertainties render this conclusion uncertain.

We group C's spectrum by 10 counts/bin for χ^2 statistics (Fig. 7), and also fit the unbinned spectrum with C-statistics (finding similar results). No single model we tried can fit this very soft spectrum, with reduced χ^2 values well above 2 (Table 2). The spectrum can be fit by a model containing two MEKAL (thermal plasma, Liedahl et al. 1995) components with the cluster absorption (to simplify fitting we fixed N_H), with temperatures of < 0.096 and > 2.3 keV. Although a double MEKAL model is often used to describe the spectra of CVs (e.g. Baskill et al. 2005), such a strong low-temperature component is rarely seen. We are aware of such components only in nova remnants (Balman 2005). Alternatively, an absorbed blackbody and MEKAL represents a simplified form of a model for polar CVs (e.g. Ramsay et al. 2004). C's spectrum is reasonably fit by a blackbody plus MEKAL model, with a blackbody temperature of 67^{+14}_{-14} eV and inferred radius of 46^{+58}_{-23} km, and a MEKAL temperature of > 3.2 keV.

3.4. Source D:

A K-S test on the unbinned lightcurve gives a prob-

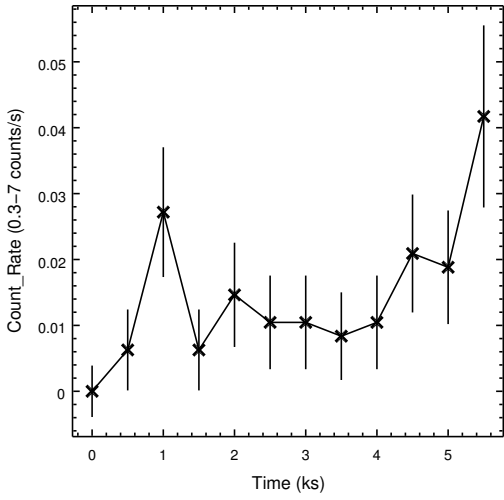


FIG. 6.— *Chandra* lightcurve of source C, 0.3-7 keV, at 500 s binning.

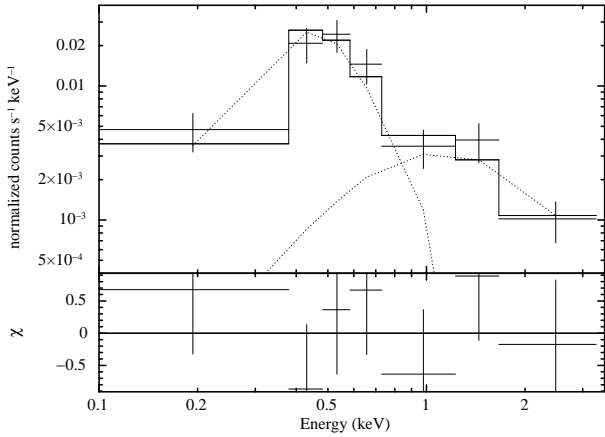


FIG. 7.— Top: *Chandra* 2008 X-ray spectrum of source C, fit by a low-temperature blackbody plus MEKAL model. Dotted lines indicate the two components (the blackbody is the lower-temperature component). Bottom: Residuals to the best fit.

ability of constancy of 0.46. The estimated luminosity from the HRC data using the ACIS power-law fit below is $L_X(0.5-10.0) = 1.1 \times 10^{33}$ ergs/s. This is comparable to the luminosity from the ACIS data, $L_X(0.5-10.0) = 8_{-3}^{+5} \times 10^{32}$ ergs/s, so no variability is apparent.

We extract a 69-count spectrum, binned with 10 counts/bin. Source D is relatively soft, with all 6 bins below 2.0 keV (Fig. 8), motivating us to freeze N_H to the cluster value. An NSATMOS model is a poor fit, but an absorbed powerlaw (photon index of $2.3_{-0.6}^{+0.4}$) is an adequate fit to the binned spectrum; a single-temperature MEKAL is a somewhat worse fit (Table 2; null hypothesis probabilities of 25% and 11% respectively). The power-law fit, however, shows residuals suggesting strong line emission around 1 keV (Fig. 8). Adding a gaussian line of zero width to the power-law fit gives a line energy of $1.03_{-0.04}^{+0.12}$ keV, but does not improve the fit by a statistically significant amount (an F-test indicates a probability of 43% that such an improvement could happen by chance). Fitting the unbinned data (using the

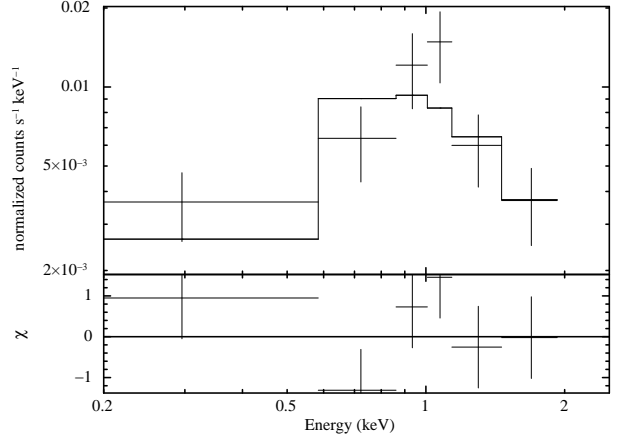


FIG. 8.— Top: *Chandra* spectrum of source D, fit to an absorbed power-law model (see text). Bottom: Residuals to the best fit.

C-statistic) with a power-law gives a slightly larger photon index ($2.7_{-0.4}^{+0.4}$), and the fraction of simulated spectra with lower C-statistic values is 97%, suggesting a relatively poor fit. (The single-temp MEKAL fit to the unbinned spectrum gives 96% of simulations with lower C-statistic values, as well.)

3.5. Faint Sources:

We detect only 15, 7, and 15 events for source E, F, and G respectively, too few for detailed spectral and timing analyses. We extract background-subtracted count rates in energy bands of 0.5-6.0 keV, 0.5-1.5 keV, and 1.5-6 keV, using the WAVDETECT regions and PIMMS to estimate unabsorbed source luminosities. While sources E and F have roughly equal numbers of soft and hard counts, all but one of source G's counts lie above 1.5 keV, suggesting strong absorption.

Using PIMMs, we estimate the unabsorbed luminosities of the faint sources in both the 0.5-1.5 keV and 1.5-6.0 keV energy bands, using an absorbed power-law of photon index 1.4. We determine the total unabsorbed luminosity from 0.5 to 6.0 keV for each source by adding the soft and hard luminosities (Table 1). We extract the counts at the ACIS WAVDETECT coordinates for each source from the HRC dataset, finding 4, 1, and 0 counts from E, F, and G respectively. These upper limits are consistent with their measured ACIS luminosities.

3.6. X-ray Color-Magnitude Diagram:

We create an X-ray color-magnitude diagram (Fig. 9) containing the sources observed in the 2008 ACIS data, by plotting the unabsorbed 0.5-6.0 keV luminosities versus the X-ray color, defined as $2.5 \log [(0.5-1.5 \text{ keV counts}) / (1.5-6.0 \text{ keV counts})]$ (Grindlay et al. 2001). We plot an X-ray color-luminosity relation for the NSATMOS model, and X-ray color predictions for power-law and MEKAL spectral models. The spectra of qLMXBs are frequently modeled with a neutron star atmosphere (e.g., NSATMOS Heinke et al. 2006b) component, with a harder power-law component with a photon index of 1-2 (Rutledge et al. 2002b), making up anywhere from < 10 to > 90% of the 0.5-10 keV flux (Jonker et al. 2004a). We plot a representative NSATMOS plus power-law model in which the power-law component contributes 50% of the 0.5-6.0 keV luminosity. Note that B's position is shifted to the left by pileup (considering its rapid variability, it is hard to correct for this).

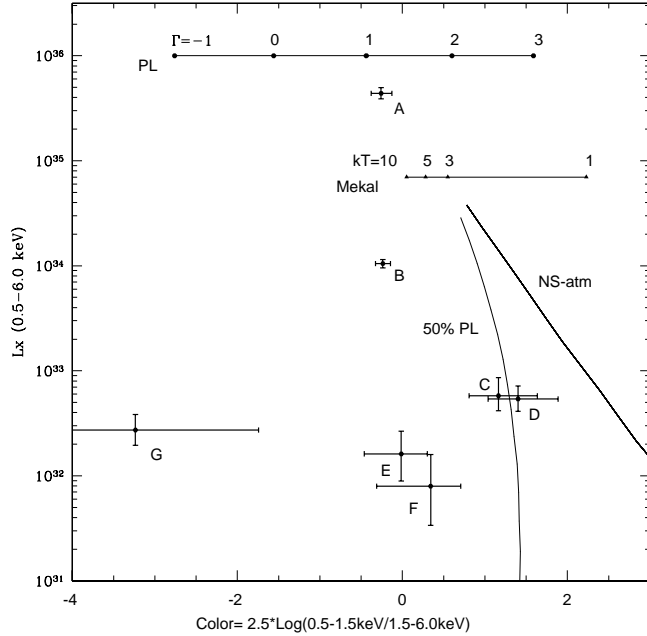


FIG. 9.— X-ray color-magnitude diagram for all sources detected in the 2008 *Chandra* ACIS-S observation. The color is defined as a function of the ratio of low-energy counts to high-energy counts. X-ray luminosities between 0.5 keV and 6.0 keV are plotted versus the color along with their respective errors. Also shown are the theoretical cooling tracks for the power-law, MEKAL, NSATMOS, and NSATMOS+power-law models. The NSATMOS+power-law model is defined such that 50% of the model’s 0.5–6 keV luminosity is produced by the power-law component.

No sources lie near the NS atmosphere cooling track, but sources C and D have colors and luminosities in the range of qLMXBs in other clusters (e.g. Pooley & Hut 2006; Heinke et al. 2006b). C’s rapid variability and unusual spectrum likely rule out a qLMXB nature for it, but D could be a qLMXB with a dominant power-law spectral component.

Surveys of X-ray sources in globular clusters indicate that most nonmagnetic CVs display hard spectra, typically consistent with MEKAL temperatures > 6 keV or colors < 0.5 (Grindlay et al. 2001; Pooley et al. 2002). Sources E, F and G are consistent with the X-ray luminosities and spectra of CVs observed in many other globular clusters (Pooley & Hut 2006; Heinke et al. 2005), though quiescent LMXBs, active binaries, and millisecond pulsars cannot be ruled out. G’s extremely hard spectrum, though based on few counts, indicates a high intrinsic absorption ($> 10^{22} \text{ cm}^{-2}$), and thus an edge-on CV (e.g. W8, W15, W33, and AKO9 in 47 Tuc, Heinke et al. 2005) or a background AGN.

4. DISCUSSION

4.1. Source B: Unusual LMXB

Source B, one of the brightest low- L_X cluster sources, can be classified as a very faint X-ray transient (VFXT). VFXTs are X-ray transients that have peak luminosities of 10^{34-36} ergs/s and quiescent luminosities at least one order of magnitude lower (Wijnands et al. 2006; Munro et al. 2005a), generally containing an accreting neutron star or black hole. Some VFXTs have “normal” outbursts as well as very faint outbursts, but it is

not clear if all do, or if VFXT behavior has a variety of causes (Degenaar & Wijnands 2010).

Fig. 3 illustrates that source B reaches peak X-ray luminosities up to $L_X(0.5-10.0 \text{ keV}) = 9 \times 10^{34}$ ergs/s and minimum $L_X < 2 \times 10^{33}$ ergs/s on timescales of minutes. B’s high peak luminosity is strong evidence that the system must contain a neutron star or a black hole, but the variability is unusual for LMXBs. Perhaps the simplest explanation for this variability is a high inclination angle, so that we observe B’s accretion disk edge-on, and our view of the central X-ray source is interrupted by structures at the accretion disk rim (White & Holt 1982; Xiang et al. 2009). Obscuration by an accretion disk should lead to changes in the N_H value, and our spectral analysis gives evidence in favor of this (section 3.2.2). Our spectral fitting requires intrinsic L_X changes along with N_H changes, which seems to argue against this explanation. However, our spectral fitting is constrained by a lack of data to only three count-rate ranges, which contain substantial variability, and we think it likely that variability also occurs on timescales shorter than we can accurately probe. These two effects could prevent us from accurately measuring how N_H changes with L_X in B’s lightcurve, and thus we cannot yet rule out that obscuration is fully responsible for the variability.

If we only see scattered light from a central source (in this picture the variability is due to obscuration of an accretion disk corona), the true isotropic X-ray luminosity could be higher than the observed luminosity, by a factor of up to 100 (e.g. Munro et al. 2005b). Thus, B could be a ‘normal’ LMXB, which would remove the difficulty of explaining its unusually low accretion luminosity. We have been awarded a deeper *Chandra* observation of NGC 6652 (50 ks, to be taken mid-2011), which should clarify the spectral variability of this source. We have also been awarded a Gemini time-series imaging observation of NGC 6652, designed to search for evidence of short periods in sources A and B suggested by previous HST imaging (Deutsch et al. 2000; Heinke et al. 2001).

4.2. Source C: A Second Polar in a Globular Cluster?

The very soft spectral component of C is unlike anything seen in quiescent LMXBs, but is consistent with the spectra of some CVs. The (low-T) blackbody + (high-T) MEKAL spectral fit suggests a polar CV nature, where the blackbody describes soft X-rays emitted from the white dwarf’s polar cap, and the MEKAL describes hard X-rays from the accretion column shock front (Ramsay & Cropper 2004). The inferred polar cap radius of 25^{+40}_{-14} km (from the blackbody spectral fit) compares well with the typical radius of an accreting pole of a WD of ~ 75 km (for a $0.6 M_\odot$ WD, Ishida et al. 1997). The spectrum and luminosity are similar to the likely polar CV X10 in the globular cluster 47 Tuc (Heinke et al. 2005), which has $L_X(0.5-6 \text{ keV}) = 2.6 \times 10^{32}$ ergs/s, and was modeled with a $kT = 53$ eV blackbody and two MEKAL plasmas of temperatures 0.39 and > 14 keV. Thus we suggest source C may be the second polar CV identified in a globular cluster. Knowing the frequency of magnetic accretion channelling in cluster CVs (by identifying magnetic CVs) is important for understanding their unusually rare outbursts (Grindlay 1999; Dobrotka et al.

2006; Ivanova et al. 2006).

Alternatively, a very low-T thermal plasma has been seen in historical novae, from the nova shell (e.g. Balman 2005). However, the nova eruption would probably have been seen if recent, or if old, the shell should have expanded to a resolvable size (e.g., the Nova Per 1901 shell would be 2.5" in radius if located in NGC 6652). Our upcoming *Chandra* observation should provide sufficiently high-quality spectra to distinguish between the spectral models discussed, and search for spectral variations over time.

4.3. Source D: unusual CV or quiescent LMXB?

Source D's luminosity and spectrum are consistent with both CVs or quiescent LMXBs. The feature of particular interest is the hint of an emission line around 1 keV. If this feature is real (which will be tested by our upcoming *Chandra* observation), it would make D a rather

odd X-ray source. There is another X-ray bright CV with a similarly strong low-energy line, the luminous CV X9 in 47 Tuc (Heinke et al. 2005).

4.4. Faint Sources

The pronounced spectral hardness of G indicates it is an edge-on CV, or a background AGN. E and F cannot be clearly classified, but as the majority of globular cluster X-ray sources with their X-ray colors and L_X are CVs (Pooley & Hut 2006), we may suggest that CVs are the most likely possibility. Deeper *Chandra* observations should detect additional sources, enabling a comparison of the amazingly rich X-ray population of this globular cluster with other globular clusters.

We acknowledge support from NASA *Chandra* grants, an NSERC Discovery Grant, and an Alberta Ingenuity New Faculty Award. We thank M. Munro for his assistance in obtaining these observations.

REFERENCES

- Balman, S. 2005, *ApJ*, 627, 933
 Baskill, D. S., Wheatley, P. J., & Osborne, J. P. 2005, *MNRAS*, 357, 626
 Brown, E. F., Bildsten, L., & Rutledge, R. E. 1998, *ApJ*, 504, L95
 Campana, S., Colpi, M., Mereghetti, S., Stella, L., & Tavani, M. 1998, *A&A Rev.*, 8, 279
 Campana, S. et al. 2002, *ApJ*, 575, L15
 Chaboyer, B., Sarajedini, A., & Armandroff, T. E. 2000, *AJ*, 120, 3102
 Clark, G. W. 1975, *ApJ*, 199, L143
 Davis, J. E. 2001, *ApJ*, 562, 575
 Degenaar, N., & Wijnands, R. 2010, *A&A*, 524, A69+
 Deutsch, E. W., Margon, B., & Anderson, S. F. 1998, *AJ*, 116, 1301
 —. 2000, *ApJ*, 530, L21
 Dobrotka, A., Lasota, J., & Menou, K. 2006, *ApJ*, 640, 288
 Gehrels, N. 1986, *ApJ*, 303, 336
 Giacconi, R., Rosati, P., Tozzi, P., & et al. 2001, *ApJ*, 551, 624
 Grindlay, J. E. 1999, in *ASP Conf. Series*, Vol. 157, Annapolis Workshop on Magnetic Cataclysmic Variables, ed. C. Hellier & K. Mukai, 377+
 Grindlay, J. E., Heinke, C. O., Edmonds, P. D., Murray, S. S., & Cool, A. M. 2001, *ApJ*, 563, L53
 Harris, W. E. 1996, *AJ*, 112, 1487
 Heinke, C. O. et al. 2010, *ApJ*, 719, 894
 Heinke, C. O., Edmonds, P. D., & Grindlay, J. E. 2001, *ApJ*, 562, 363
 Heinke, C. O., Grindlay, J. E., Edmonds, P. D., Cohn, H. N., Lugger, P. M., Camilo, F., Bogdanov, S., & Freire, P. C. 2005, *ApJ*, 625, 796
 Heinke, C. O., Grindlay, J. E., Lugger, P. M., Cohn, H. N., Edmonds, P. D., Lloyd, D. A., & Cool, A. M. 2003, *ApJ*, 598, 501
 Heinke, C. O., Rybicki, G. B., Narayan, R., & Grindlay, J. E. 2006a, *ApJ*, 644, 1090
 Heinke, C. O., Wijnands, R., Cohn, H. N., Lugger, P. M., Grindlay, J. E., Pooley, D., & Lewin, W. H. G. 2006b, *ApJ*, 651, 1098
 Ishida, M., Matsuzaki, K., Fujimoto, R., Mukai, K., & Osborne, J. P. 1997, *MNRAS*, 287, 651
 Ivanova, N., Heinke, C. O., Rasio, F. A., Taam, R. E., Belczynski, K., & Fregeau, J. 2006, *MNRAS*, 367, 1073
 Jonker, P. G., Galloway, D. K., McClintock, J. E., Buxton, M., Garcia, M., & Murray, S. 2004a, *MNRAS*, 354, 666
 Jonker, P. G., Wijnands, R., & van der Klis, M. 2004b, *MNRAS*, 349, 94
 Katz, J. I. 1975, *Nature*, 253, 698
 Liedahl, D. A., Osterheld, A. L., & Goldstein, W. H. 1995, *ApJ*, 438, L115
 Mukai, K., & Smale, A. P. 2000, *ApJ*, 533, 352
 Munro, M. P., Lu, J. R., Baganoff, F. K., Brandt, W. N., Garmire, G. P., Ghez, A. M., Hornstein, S. D., & Morris, M. R. 2005a, *ApJ*, 633, 228
 Munro, M. P., Pfahl, E., Baganoff, F. K., Brandt, W. N., Ghez, A., Lu, J., & Morris, M. R. 2005b, *ApJ*, 622, L113
 Noyola, E., & Gebhardt, K. 2006, *AJ*, 132, 447
 Parmar, A. N., Oosterbroek, T., Sidoli, L., Stella, L., & Frontera, F. 2001, *A&A*, 380, 490
 Pooley, D., Homan, J., Heinke, C., Linares, M., Altamirano, D., & Lewin, W. 2010, *The Astronomer's Telegram*, 2974, 1
 Pooley, D., & Hut, P. 2006, *ApJ*, 646, L143
 Pooley, D. et al. 2002, *ApJ*, 569, 405
 Predehl, P., Hasinger, G., & Verbunt, F. 1991, *A&A*, 246, L21
 Ramsay, G., & Cropper, M. 2004, *MNRAS*, 347, 497
 Ramsay, G., Cropper, M., Mason, K. O., Córdova, F. A., & Priedhorsky, W. 2004, *MNRAS*, 347, 95
 Rutledge, R. E., Bildsten, L., Brown, E. F., Pavlov, G. G., & Zavlin, V. E. 2002a, *ApJ*, 578, 405
 —. 2002b, *ApJ*, 577, 346
 Sidoli, L., La Palombara, N., Oosterbroek, T., & Parmar, A. N. 2008, *A&A*, 488, 249
 Sidoli, L., Parmar, A. N., Oosterbroek, T., Stella, L., Verbunt, F., Masetti, N., & Dal Fiume, D. 2001, *A&A*, 368, 451
 Tarana, A., Bazzano, A., Ubertini, P., & Federici, M. 2007, in *ESA Special Pub.*, Vol. 622, 437
 Verbunt, F., & Lewin, W. H. G. 2006, in "Compact Stellar X-ray Sources", ed. W. Lewin & M. van der Klis, Cambridge U. Press
 White, N. E., & Holt, S. S. 1982, *ApJ*, 257, 318
 Wijnands, R., Heinke, C. O., Pooley, D., Edmonds, P. D., Lewin, W. H. G., Grindlay, J. E., Jonker, P. G., & Miller, J. M. 2005, *ApJ*, 618, 883
 Wijnands, R. et al. 2006, *A&A*, 449, 1117
 Xiang, J., Lee, J. C., Nowak, M. A., Wilms, J., & Schulz, N. S. 2009, *ApJ*, 701, 984
 Zavlin, V. E., Pavlov, G. G., & Shibano, Y. A. 1996, *A&A*, 315, 141

TABLE 1
Sources in NGC 6652 Field

Name	SOURCE CXOGLB J	R.A.	ERR	DECL.	ERR	COUNTS (0-10 keV)	L_X (10^{32} ergs s $^{-1}$)			
							(0.5-1.5 keV)	(1.5-6 keV)	(0.5-6 keV)	
A	183543.7-325927	18:35:43.69	0.02	-32:59:26.5	0.5	462 ^a	1574 ⁺⁵³³ ₋₃₈₆	2813 ⁺³¹² ₋₃₁₀	4386 ⁺⁵⁹⁹ ₋₅₀₇	
B	183544.6-325938	18:35:44.567	0.001	-32:59:38.36	0.02	680	27 ⁺⁷ ₋₅	77 \pm 8	105 ⁺¹⁰ ₋₉	
C	183545.8-325923	18:35:45.755	0.003	-32:59:23.21	0.04	90	3.9 ^{+0.9} _{-0.9}	1.9 ^{+2.6} _{-1.1}	5.8 ^{+2.8} _{-1.6}	
D	183545.6-325926	18:35:45.648	0.004	-32:59:26.10	0.05	73	3.3 ^{+0.8} _{-0.7}	2.1 ^{+1.8} _{-0.9}	5.4 ^{+1.8} _{-1.3}	
E	183546.2-325929	18:35:46.206	0.010	-32:59:29.26	0.09	15	0.47 ^{+0.28} _{-0.19}	1.2 ^{+0.8} _{-0.5}	1.6 ^{+1.0} _{-0.7}	
F	183547.8-325920	18:35:47.777	0.004	-32:59:19.84	0.15	7	0.27 ^{+0.23} _{-0.14}	0.53 ^{+0.37} _{-0.32}	0.80 ^{+0.80} _{-0.46}	
G	183548.8-325921	18:35:48.816	0.009	-32:59:21.13	0.10	15	0.05 ^{+0.17} _{-0.05}	2.7 ^{+0.9} _{-0.7}	2.7 ^{+1.1} _{-0.8}	

NOTE. — Positions (with relative errors, not including systematic uncertainties on the *Chandra* astrometry), total counts, and inferred luminosities for NGC 6652 sources.

^a: From readout streak.

TABLE 2
Spectral Fits

Src	Model	N_H (10^{20} cm $^{-2}$)	Γ	kT keV	χ^2_v/dof	L_X
A	POW	27 ⁺¹⁰ ₋₈	1.7 ^{+0.3} _{-0.2}	-	0.87/6	5.8 ^{+0.8} _{-0.7} $\times 10^{35}$
B	POW	5 ⁺⁶ ₋₀	1.3 ^{+0.2} _{-0.2}	-	0.70/18	1.7 ^{+0.2} _{-0.2} $\times 10^{34}$
B	POW+NSATMOS	5 ⁺⁸ ₋₀	1.2 ^{+0.2} _{-0.2}	-	0.736/17	1.7 ^{+0.2} _{-0.2} $\times 10^{34}$
-	NSATMOS	-	-	10 ⁺¹⁰⁰ ₋₁₀	-	< 7 $\times 10^{32}$
C	POW	(5)	5.2	-	3.14/5	4.1 $\times 10^{32}$
C	MEKAL	(5)	-	0.14	6.24/5	5.6 $\times 10^{32}$
C	MEKAL+MEKAL	(5)	-	0.08 ^{+0.015} ₋₀	0.45/3	1.1 ^{+0.9} _{-0.5} $\times 10^{33}$
-	2nd MEKAL	-	-	> 2	-	7.3 ^{+2.8} _{-4.3} $\times 10^{32}$
C	MEKAL+BBODY	(5)	-	> 3.3	1.00/3	1.2 ^{+0.1} _{-0.5} $\times 10^{33}$
-	BBODY	-	-	0.067 ^{+0.013} _{-0.013}	-	3.1 ^{+1.2} _{-1.3} $\times 10^{32}$
D	POW	(5)	2.3 ^{+0.6} _{-0.6}	-	1.33/4	8 ⁺⁵ ₋₃ $\times 10^{32}$
D	MEKAL	(5)	-	2 ⁺⁵ ₋₁	1.88/4	6.8 ^{+6.2} _{-2.5} $\times 10^{32}$
D	NSATMOS	(5)	-	0.1	2.3/5	4.3 $\times 10^{32}$
D	POW+GAU	(5)	2.3 ^{+0.7} _{-0.7}	-	1.14/2	8 ⁺⁵ ₋₃ $\times 10^{32}$
-	GAU	-	1.03 ^{+0.12} _{-0.04}	-	-	5 ⁺⁵ ₋₅ $\times 10^{31}$

NOTE. — Spectral fits to NGC 6652 sources (see text for details). Errors are 90% confidence for a single parameter, and are not computed if $\chi^2_v > 2$. Luminosities are unabsorbed in erg s $^{-1}$ for 0.5-10 keV. Two-component models are continued on a second line (omitting the source name in the first column), with the total luminosity on the first line and the second component's luminosity individually on the second line. All models include PHABS; for faint, soft sources, we have fixed the N_H to the cluster value.

TABLE 3
Count-rate-Resolved Spectral Fits to B

Source	Model	N_H (10^{20} cm^{-2})	Γ	χ^2_v/dof	L_X ergs/s
Allowing PL norm and index to vary					
B (High)	PHABS(POW)	(5)	$1.5^{+0.2}_{-0.2}$	0.84/36	$5.1^{+1.1}_{-1.0} \times 10^{34}$
B (Med)	$1.3^{+0.3}_{-0.3}$...	$2.7^{+0.7}_{-0.7} \times 10^{34}$
B (Low)	$1.0^{+0.2}_{-0.2}$...	$1.2^{+0.2}_{-0.2} \times 10^{34}$
Allowing PL norm and N_H to vary					
B (High)	PHABS(POW)	$5.0^{+3.3}_{-0.9}$	$1.4^{+0.7}_{-0.4}$	0.83/37	$5.5^{+1.1}_{-1.0} \times 10^{34}$
B (Med)	...	$5.9^{+7.6}_{-0.9}$	$2.4^{+0.5}_{-0.5} \times 10^{34}$
B (Low)	...	22^{+12}_{-9}	$1.1^{+0.2}_{-0.2} \times 10^{34}$

NOTE. — Spectral fits to NGC 6652 B, split by count-rate (see text). Errors are 90% confidence for a single parameter. Luminosities are unabsorbed in erg s^{-1} for 0.5-10 keV.